Earth and Planetary Science Letters 283 (2009) 38–47

Contents lists available at ScienceDirect

Earth and Planetary Science Letters

journal homepage: www.elsevier.com/locate/epsl

Homogenization processes in silicic magma chambers by stirring and mushification (latent heat buffering)

Christian Huber [a,*], Olivier Bachmann [b], Michael Manga [a]

[a] Department of Earth and Planetary Science, University of California, Berkeley, United States
[b] Department of Earth and Space Sciences, University of Washington, Seattle, United States

ARTICLE INFO

Article history:
Received 16 September 2008
Received in revised form 9 March 2009
Accepted 10 March 2009
Available online 23 April 2009

Editor: T.M. Harrison

Keywords:
magma chamber
convective stirring
homogenization
crystal mush
latent heat buffering
silicic magmas

ABSTRACT

Heterogeneities in crustal magma chambers are generated by incomplete mixing of different batches of magmas, precipitation or remelting of solids ~10–20% denser than surrounding liquids at cooling/heating boundaries, and by liquid extraction from more dense crystalline residues. Volcanic eruptions commonly sample that heterogeneity as many deposits from large explosive events show gradients in composition, crystallinity and temperature. However, some of the most viscous of all magmas – crystal-rich rhyolites–dacites and large silicic plutons – are, in contrast, strikingly homogeneous. This observation is in stark contradiction to the common assumption that the main homogenizing process in magma chambers is mechanical mixing by convection.

The timescale for convective stirring is governed by flow velocities. The faster the convective currents, the more rapidly mixing occurs. However, it is the total amount of strain that determines whether homogeneity can be attained. Here, we show that convecting magma body needs 5–10 overturns following the introduction of heterogeneities to be homogenized to lengthscales at which diffusion is effective, irrespective of the vigor of the convection. For heterogeneities that are discrete in time and space and mechanically passive (such as patches of magmas with slightly different characteristics), the threshold of 5–10 overturns can potentially be reached if enough time is allowed for the system to convect. For heterogeneities that are continuously re-established or introduced by the convective process itself (such as density instabilities generated by crystallization at the cooling boundaries of magma chambers), convective stirring is unable to produce complete homogeneity. Therefore, to explain the low variability in major element whole-rock composition in crystal-rich dacitic/rhyolitic ignimbrites and silicic plutons, we propose that another mechanism of homogenization acts to decrease thermal, and related crystallinity variability at high crystal fraction (>50 vol.%). It is induced by latent heat buffering of silicic magmas close to the haplogranitic eutectic, and leads to the rapid equilibration of temperature (and crystal fraction) throughout the magma reservoir. As this process drives the magma body towards a uniformly high crystallinity ("crystal mush"), we refer to it as "mushification". Nevertheless, the homogeneity of both large crystal-rich silicic ignimbrites and granites also require (1) incremental growth dominated by addition of magma batches that are compositionally similar to reach the observed large sizes without inducing unmixable chemical heterogeneities and (2) some late convective stirring at high crystallinity to explain the dispersal of externally derived crystalline material, e.g. xenocrysts and antecrysts. Late mechanical mixing mostly occurs at high crystallinity (~30–50 vol.% crystals) following the intrusion of hotter magmas (and gas) from below, triggering whole-reservoir convective overturn without introducing new significant gradients.

1. Introduction

The compositional diversity of Earth's magmatic rocks can seem bewildering (e.g., Bowen, 1992) and is unique among terrestrial planets (Campbell and Taylor, 1988). This compositional array requires that a number of processes act to generate heterogeneities from initially fairly homogeneous (at least in major-elements) basaltic melts produced by melting the mantle. On Earth, two main mechanisms can generate chemical heterogeneities in magmas: (1) "distillation" processes caused by phase separation in a gravity field due to variable densities, either during partial melting or fractional crystallization and (2) coarse and incomplete mixing of chemically different magma batches. Both trends of heterogenization are commonly preserved in erupted rocks, and have been inferred to record respectively (1) progressive unmixing and (2) arrested homogenization (Eichelberger et al., 2000).

* Corresponding author.
E-mail address: chuber@seismo.berkeley.edu (C. Huber).

0012-821X/$ – see front matter © 2009 Elsevier B.V. All rights reserved.
doi:10.1016/j.epsl.2009.03.029

In this world of magmas where heterogeneity is the rule, it is surprising that some of the most viscous magma bodies (such as granitic plutons and crystal-rich, dacitic ignimbrites referred to as the "Monotonous Intermediates" (MI); Hildreth (1981)) display remarkable homogeneity in temperature, crystallinity and major-element composition at the hand sample scale (e.g., Bateman and Chappell, 1979; Whitney and Stormer, 1985; Bachmann et al., 2002). As the efficiency of mixing is commonly expressed as a function of the Reynolds number ($Re = uH/\nu$) (e.g., Jellinek and Kerr, 1999), which is inversely proportional to kinematic viscosity ($\nu = \mu/\rho$, where μ is the dynamic viscosity) and depends both on the fluid velocity u and fluid layer thickness H, the most viscous magmas should be expected to be among the most heterogeneous. Moreover, although thermal and compositional convection clearly occurs in magma reservoirs (Grout, 1918) and can act as an homogenizer (e.g., Whitney and Stormer, 1985; Oldenburg et al., 1989; Lindsay et al., 2001; Christiansen, 2005), it has been shown that convective stirring in magma reservoirs is prone to generate stratification (Chen and Turner, 1980; McBirney, 1980; McBirney et al., 1985; Bergantz and Ni, 1999; Jellinek and Kerr, 1999; Jellinek et al., 1999).

Using scaling laws and parameterized dynamical models of natural magmas, we analyse the conditions in which mixing by convection is efficient. We investigate the role of chemical and thermal buffering close to the haplogranitic eutectic at near-solidus conditions, when convection can no longer act as an efficient stirrer. We present theoretical arguments and a simplified magma chamber model to illustrate these processes.

2. Convective stirring

The challenges posed by understanding convective dynamics of magma chambers has led to long-standing controversies (e.g., Sparks et al., 1984; Marsh, 1989a,b; Sparks, 1990; Bergantz, 1992; Koyaguchi and Kaneko, 1999, 2001). Assessing convective vigor and evolution of natural magmas requires a reasonable model of the evolution of viscosity and crystallinity over time in a open system that exchanges heat and mass with its surroundings, both wall rocks and influx of more primitive magmas. In high viscosity fluids such as crystal-rich silicic (>65–70 wt.% SiO_2) magmas with viscosities from about 10^4 Pa s to 10^{10} Pa s (Scaillet et al., 1998), stirring any heterogeneities in composition, temperature, and crystallinity by convection is unavoidably slow and difficult.

To constrain the conditions necessary for these magmas to reach homogeneity defined here as the stage at which the length scale of heterogeneities in a body of magma is comparable to the diffusion length for the scalar field of interest; (e.g., Coltice and Schmalzl, 2006), we designed a parameterized numerical model for the cooling and crystallization of a canonical, closed system, magma chamber. For the sake of simplicity in the following development, we assume that the diffusing scalar field (either composition, temperature or crystallinity) is passively advected by the convection flow-field. This assumption is reasonable for temperature and composition away from the solidus temperature and for crystallinity in viscous silicic magmas as the settling velocity is generally negligible compared to the average convective flow velocity (Sparks et al., 1984; Martin and Nokes, 1989; Koyaguchi et al., 1990; Burgisser et al., 2005).

2.1. A simplified model of monotonically cooling magma chamber

It is widely accepted that magma chamber cooling rate is "regulated" by heat transfer to the host rocks, i.e., in a cooling system, the magma cannot transfer more heat than the rocks can remove as this would lead to superheating the host rocks and melting of large portions of chamber wall-rock (Carrigan, 1988). Therefore, even a simplified model of magma chamber cooling, such as the one presented here, must account for the heat transfer across the rock layers above the chamber.

We solve, here, the one-dimensional heat diffusion equation

$$\frac{\partial T}{\partial t} = \kappa_r \frac{\partial^2 T}{\partial z^2}, \tag{1}$$

where T is the temperature, κ_r is the thermal diffusivity of the host rocks and z is the depth from the surface. We use Dirichlet boundary conditions (temperature specified) using an implicit finite difference method (Backward Euler). The temperature at the surface ($z = 0$) is fixed on one side of the domain and the temperature of the convecting magma is calculated on the other side ($z = D$, D being the depth at which the chamber lies), where we account for a rigid thermal boundary layer, hereafter called the lid, through which the temperature gradient is assumed to be constant (Davaille and Jaupart, 1993, 1994). The initial condition is a specified geothermal gradient (30 °C/km) across the domain with the initial temperature of the chamber $T = T_i$ at $z = D$ (see Fig. 1 and Appendix A).

We then solve the diffusion equation, and the heat flux at the boundary between the magma chamber and the host rock q_{out} is used to update the magma temperature in the convecting layer according to the following scheme: q_{out} has to match the heat flux out of the magma chamber cooling by convection and the heat released by crystallization.

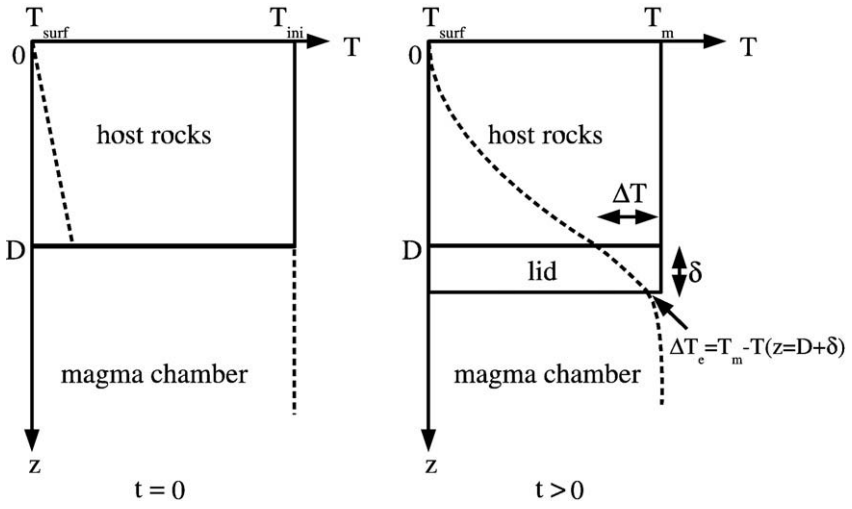

Fig. 1. Temperature profile as function of depth.

The crystallinity χ is a complicated function of temperature in silicic melts and we simplify it by assuming a smooth relationship

$$\chi(T) = 1 - \left(\frac{T - T_{sol}}{T_{liq} - T_{sol}}\right)^b, \quad 0 < b < 1. \tag{2}$$

An exponent b close to 0 characterizes systems in which the majority of the melt crystallizes in a narrow range of temperature just above the solidus, as expected for eutectic systems. χ_{cr} is the critical crystallinity at which a suspension behaves like a solid. Fig. 5 shows the different crystallinity-temperature relationships for different values of the power–law exponent b. We assume, here, $\chi_{cr} = 60\%$. More details about the cooling model for the canonical magma chamber are given in Appendix A. The set of parameters used for this calculation are listed in Table 1.

The validity of this simple cooling model is limited to relatively low crystal fractions, below the rheological lock-up that occurs around $\chi \simeq 50$ vol.% crystals (Marsh, 1981; Vigneresse et al., 1996; Petford, 2003). The formation of large-scale crystal networks will introduce a yield strength at lower volume fractions (e.g., Philpotts et al., 1998; Hoover et al., 2001; Saar and Manga, 2002; Caricchi et al., 2007; Champallier et al., 2008) and therefore modify the rheology of the magma at low Ra. However, as we consider homogenization by mechanical stirring to be most efficient at low crystal fractions ($\chi < 20\%$), we neglect a finite yield strength.

2.2. Stirring time

For large wavelength heterogeneities, the stretching induced by shear strain $\dot{\epsilon}$ dominates and leads to a deformation proportional to $(\dot{\epsilon} t)^{-1}$. Once the heterogeneities have been reduced to smaller sizes, normal strain accounts for the majority of the deformation, which becomes proportional to $\exp(-2\dot{\epsilon} t)$ (Olson et al., 1984; Ottino, 1990). Following Coltice and Schmalzl (2006), for steady-state convection, we can relate the stirring time to the strain rate

$$\tau_m = \frac{1}{2\dot{\epsilon}} log\left(\frac{\dot{\epsilon} H^2}{D}\right) \tag{3}$$

where $\frac{H^2}{D}$ is the diffusion timescale of interest in the mixing process. The dependence of the average strain-rate on the Rayleigh number (ratio of advective to diffusive timescales, defined in the Appendix A, Eq. (27) was investigated by Coltice and Schmalzl (2006) who found that:

$$\dot{\epsilon} = 0.023 \frac{\kappa}{H^2} Ra^{0.685}. \tag{4}$$

This correlation has been calculated for $10^3 \leq Ra \leq 10^9$, however large magma bodies are expected to have $Ra > 109$ at early stages. As we show in Fig. 2, the rapid cooling induced by the sharp initial temperature contrast between the magma and host rocks and the small boundary layer thickness pushes the convective magma within the range of Ra studied by Coltice and Schmalzl (2006) after about 100 years. According to this relationship, the spatial fluctuations of the velocity field (Root Mean Square—RMS–velocity) in the convecting chamber is given by

$$u = 0.023 \frac{\kappa}{H} Ra^{0.685}. \tag{5}$$

From boundary-layer theory (e.g. Turcotte and Schubert, 2002),

$$\dot{\epsilon}_{BL} = 0.271 \frac{\kappa}{H^2} Ra^{2/3}, \tag{6}$$

and consequently,

$$u_{BL} = 0.271 \frac{\kappa}{H} Ra^{2/3}, \tag{7}$$

where the subscript BL refers to values in the boundary layer.

The product of the stirring time (τ_m) and the RMS velocity, normalized by the thickness of the chamber H, gives an estimate of the total strain experienced by the fluid to reach a point where molecular diffusion takes over to further homogenize the system at a given Ra our definition of homogeneity. We refer to this measure as *the number of overturns* experienced by the fluid. Fig. 3(b) shows that the number of overturns required to reach a well-stirred fluid is largely invariant with respect to Ra (varies less than an order of magnitude, between 1 and 10, over 8 orders of magnitude of Ra). We emphasize that using thermal diffusivities or chemical diffusivities for silicate magmas, the latter being up to 6–7 orders of magnitude slower than the former does not lead to major differences (less than an order of magnitude) in the number of overturns because the stirring time τ_m is a function of $\log(1/D)$.

Using the number of overturns as a first order proxy for the stirring efficiency of some passively advected scalar field has an advantage over estimates of the stirring time based on the strain rate or the Reynolds number. Average strain rate is only defined for constant Rayleigh numbers, or at least for a dynamical evolution that occurs over a timescale much longer than τ_m. This condition is continuously violated in real magma chambers, where the cooling rate ranges over many orders of magnitude (see Fig. 4, right, for the simplified model) or when injections of new, hot, magma can occur over short times. The invariance of the number of overturns on Ra (roughly between 5 and 10 overturns for any realistic Ra), and therefore on the temporal evolution of a convective fluid offers, to a first order, a way to estimate the efficiency of stirring independent of the time-dependent convective history of the body.

As the total strain required to mix a passive tracer should be invariant, we attribute the small variation in number of overturns (Fig. 3(b)) to the chaotic mixing at high Ra due to the transient evolution of the position of stagnation points where the most effective stirring occurs. We also note that the number of overturns needed to achieve significant stirring is similar using results from boundary layer analysis. It is also important to emphasize that the mechanical stirring considered here is valid for heterogeneities and bulk magma having similar viscosities, which is not always a good approximation for natural systems (e.g., crystal-rich plumes; Bergantz and Ni, 1999), or for injected batches of magma (Sparks and Marshall, 1986). However, Manga (1996) showed that this effect is easily accounted for by rescaling the strain rates by $1 + \lambda$, where λ is the viscosity ratio of the bulk magma and heterogeneity.

Table 1
Parameter values.

D	Magma chamber depth	2 km
H	Magma chamber thickness	500 m
V	Magma chamber volume	10^3 km^3
T_i	Initial temperature of magma	950 °C
T_{liq}	Temperature of liquidus	1000 °C
T_{sol}	Temperature of solidus	700 °C
G	Initial geothermal gradient	30 °C/km
μ_0	Viscosity of melt at $T = T_{ini}$	10^4 Pa s
α_T	Thermal expansion coefficient	3×10^{-5} °C^{-1}
k	Thermal conductivity of host rocks	2 W/m K
ρ_r	Density of host rocks	2800 kg/m^3
c_{pr}	Specific heat of host rocks	1400 J/kg °C
χ	Crystallinity in volume percent	
ρ_m	Density of the melt	2400 kg/m^3
ρ_c	Density of the crystals	2600 kg/m^3
L	Latent heat of crystallization	2.7×10^5 J/kg

3. Consequences of magma stirring by convection

To understand how upper crustal silicic magmas are stirred by convection, we examine the two most common scenarios: (1) a

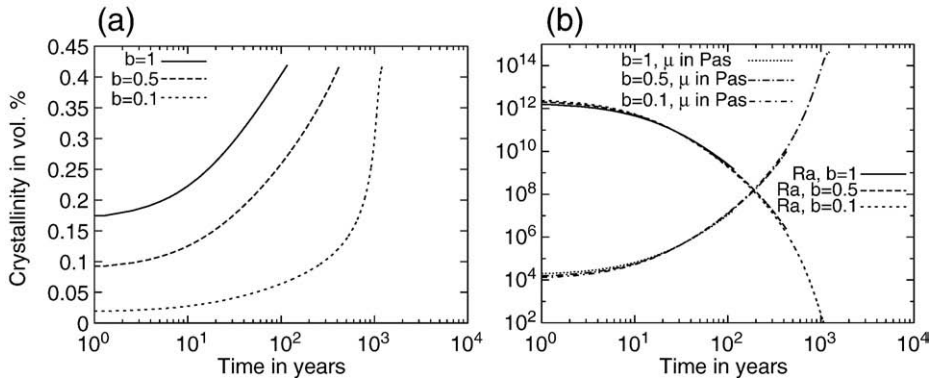

Fig. 2. (a) Evolution of the crystallinity. (b) Evolution of the Rayleigh number and dynamic viscosity of the magma as function of cooling time, using again parameters listed in Table 1.

cooling and chemically-closed system and (2) a chemically open system (with possible waxing and waning of the temperature field), with reintrusion from below.

In the first situation, an initially crystal-poor magma body will become heterogeneous with time (Bergantz and Ni, 1999). Cooling induces the crystallization of dense solids at the margins of the magma body, and generates compositionally less dense residual liquids. Crystal-rich plumes then develop at the roof of the magma chamber, and entrain dense material to the floor. This situation will lead to a low potential energy configuration once the convective motion (or kinetic energy) is no longer vigorous enough to work efficiently against a stable density layering with dense crystals at the floor and low density melts at the roof. However, the differences in temperature, crystallinity or composition between the boundary layer and the main magma body (causing the negative buoyancy and the plumes) decrease with time. For example, focusing on crystallinity, the difference in crystal content between the dense crystal-rich plumes forming at the roof and the bulk magma is greatest in the early stages of cooling when the bulk magma is close to the liquidus (crystal-free), but as cooling proceeds, the average crystallinity in the magma chamber increases and the crystallinity heterogeneity introduced from the boundary layers decreases. Stirring also becomes less efficient because the viscosity of the magma is a strong function of the crystallinity.

The second situation (chemically open system with re-intrusion from below) branches out in two different cases. The new influx of magma can be either (1) compositionally similar, but hotter and less crystalline (therefore less dense) or (2) more mafic (hotter but more dense) than the ambient magma. As for the case of closed-system cooling, intruding less crystalline (less dense, but compositionally similar) magma from below, is also expected to lead to a gradient in crystallinity. The Jellinek and Kerr (1999) laboratory experiments, in which a low density fluid with variable viscosity is introduced from below into a more dense ambient fluid, clearly demonstrate the generation of vertical gradients in density and composition in situations where the intruding fluid is less viscous. Injecting a volatile-rich layer below an initially homogeneous magma batch will also lead to a stratification (Huppert et al., 1982; Ruprecht et al., 2008). In the other magmatic intrusion scenario (hotter, but more dense mafic magma), the situation is gravitationally stable and little to no chemical mixing is induced except for the dispersal of some mafic enclaves. This "underplating" of hot magma, however, is prone to reheat and stir the overlying silicic reservoir, which will also introduce a gradient in temperature and crystallinity by sending low crystallinity plumes into an overlying more crystalline and cooler reservoir (e.g., Couch et al., 2001).

The growing stratification in most magmatic situations arises because the source of heterogeneity is itself the driving force of convection. Natural convection is due to the presence of a positively or negatively buoyant boundary layer that becomes gravitationally unstable under the influence of temperature, crystallinity or composition differences. These boundary layers are thus regions of anomalous temperature, crystallinity or composition with respect to the rest of the magma stored in the chamber and gravity currents generated by the destabilization of boundary layers bring heterogeneities into the bulk magma. As argued in Section 2, efficient stirring of new heterogeneities requires about 5–10 overturns, but a single episode of destabilization of a boundary layer leads to no more than a single overturn. Hence, convection is only able to partially stir the new heterogeneities that it introduces before reaching a stable configuration, particularly in viscous systems characterised by low Re numbers. Convection therefore has the dual nature of being a source of heterogeneity for the field responsible for the density difference and a sink of heterogeneity for every field passively advected by the flow.

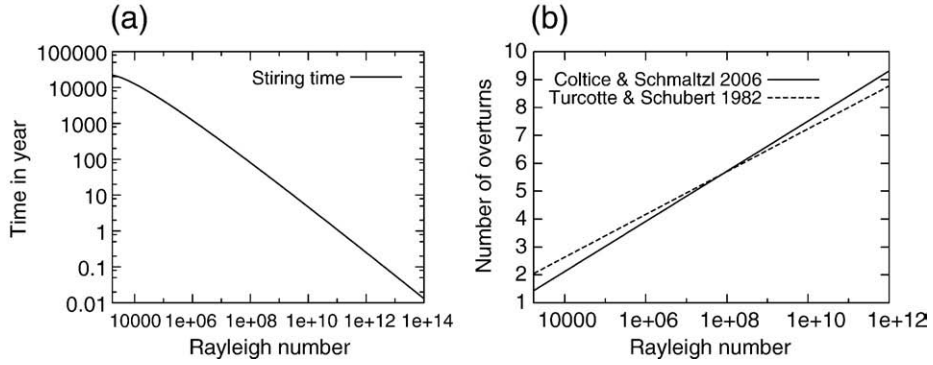

Fig. 3. (a) Stirring time from Eq. (3). (b) Comparison of the total number of overturns to reach a well-stirred chamber obtained from the two correlations cited in the text.

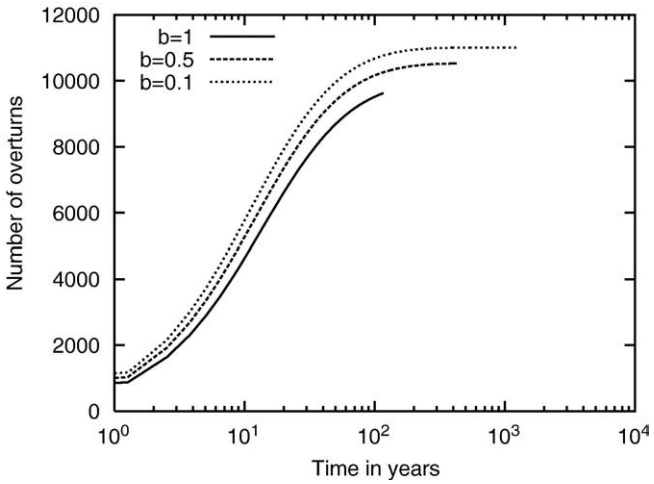

Fig. 4. Cumulative count of the number of overturns in the system described in Table 1. Note the decrease of the mixing potential once the viscosity has increased enough to damp efficiently the system.

Despite the apparent incapacity of convection to efficiently stir heterogeneities in magma chambers, many large, crystal-rich volcanic units and granitoids are strikingly homogeneous in major-element composition at least to the accuracy of available petrological probes (e.g. Lindsay et al., 2001; Bachmann et al., 2002; Charlier et al., 2007). The fact that they are crystal-rich, and thus even more viscous than near-liquidus magmas, suggests that mechanical mixing is not the only important homogenising agent in such systems. We discuss next alternative mechanisms to make these high-viscosity systems appear uniform in temperature and composition.

4. "Mushification" by near-eutectic latent heat buffering

Large silicic magma bodies appear to spend most of their life above the solidus at high crystallinity, in a so-called "crystal mush" (Koyaguchi et al., 1990; Bachmann et al., 2007). We therefore propose that homogenization of temperature and crystallinity in silicic magmas occurs by a process other than mechanical mixing. It involves temperature buffering close to the magma solidus as it reaches near-eutectic conditions of the haplogranite ternary. We present a conceptual model based on the energy budget in the magma body, where the temperature field evolves according to heat transport (mostly by diffusion at high crystallinity) and latent heat release by crystallization. We show that the discontinuous behavior of the melt fraction function with respect to temperature close to the solidus in silicic magmas requires that heat transfer balances the latent heat released, or in other words, that the cooling rate converges to zero close to the solidus. We show that two patches of magma, which start at different temperatures, will tend to converge towards the same temperature once they reach near-eutectic conditions. Latent heat buffering also leads to homogenization of crystallinity throughout the chamber.

4.1. Cooling timescale close to the solidus

Using a volume integral description of energy conservation in a cooling body undergoing solidification, and neglecting viscous dissipation, we obtain

$$\int_V \frac{\partial T}{\partial t} \mathrm{d}V + \int_V \nabla \cdot \mathbf{q}\, \mathrm{d}V = \int_V \frac{L}{c}\frac{\partial f}{\partial t} \mathrm{d}V \tag{8}$$

where $\mathbf{q}$ is the heat flux, combining both diffusion and advection, L is the latent heat of solidification, c the specific heat and f is the melt fraction. The melt fraction is a function of temperature, assuming that pressure and composition do not vary much. Using the chain rule,

$$\frac{\partial f}{\partial t} = \frac{\partial f}{\partial T}\frac{\partial T}{\partial t}. \tag{9}$$

We now need a suitable relationship between the melt fraction and the temperature. For a silicate melt at the eutectic, the melt fraction has a discontinuity at the solidus temperature which does not allow us to model the cooling evolution with the simple model described by Eq. (8). We therefore choose a continuous parametric function that shares the three main properties

$$f(T_{\mathrm{sol}}) = 0 \tag{10}$$

$$f\left(T_{\mathrm{liq}}\right) = 1 \tag{11}$$

$$lim_{(T\to T_{\mathrm{sol}})}\frac{\partial f}{\partial T} \to \infty. \tag{12}$$

These constraints are satisfied by functions of the form

$$f(T) = \left(\frac{T - T_{\mathrm{sol}}}{T_{\mathrm{liq}} - T_{\mathrm{sol}}}\right)^b, \quad 0 < b < 1. \tag{13}$$

Fig. 5 shows different melt fraction–temperature relationships using Eq. (13) with three different exponents b (hereafter referred to as the "eutectic exponent"). We argue that, although very simplified, this single free parameter parameterization of the temperature–crystallinity relationship shares the main characteristics of the calculated relationships for near-eutectic magmas and allows an straight-forward analytical investigation of cooling rates close to the solidus of these magmas.

Rewriting Eq. (8) with this choice of parametric melt fraction–temperature relationship, we obtain

$$\int_V \frac{\partial T}{\partial t} \mathrm{d}V + \int_V \nabla \cdot \mathbf{q}\, \mathrm{d}V = \int_V \frac{Lb}{c\left(T_{\mathrm{liq}} - T_{\mathrm{sol}}\right)}\left(\frac{T - T_{\mathrm{sol}}}{T_{\mathrm{liq}} - T_{\mathrm{sol}}}\right)^{b-1}\frac{\partial T}{\partial t} \mathrm{d}V. \tag{14}$$

The right-hand side of this equation diverges as the system cools and approaches the solidus temperature, unless the time derivative of

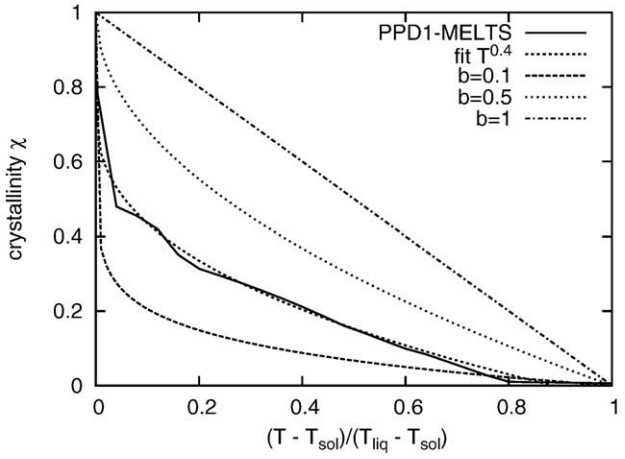

Fig. 5. The functional parameterization of eutectic melt fraction–temperature relationships. As the exponent b (Eq. (13)) decreases close to zero, most of the crystallization occurs over a narrower range of temperatures and will asymptotically approach a step function for $b = 0$. The melt fraction temperature curve calculated with MELTS (Ghiorso and Sack, 1995) for the whole composition of the Pagosa Peak Dacite (Fish Canyon magma body) from Bachmann et al. (2002) is shown for reference.

temperature converges to zero faster than $(T-T_{sol})^{b-1}$ diverges. This constraint implies that when the system approaches the solidus, temperature is buffered and the cooling rate becomes small. This is a consequence of the balance between latent heat release close to the solidus and the heat fluxed out of the system. In cases where the flow has not totally ceased, the decrease in cooling rate may allow more time for low *Re* stirring. Close to eutectic conditions, however, where advective heat transfer can be neglected (low Peclet number), we have

$$\left|\kappa\nabla^2 T\right| = \left|\frac{Lb}{c\left(T_{liq}-T_{sol}\right)}\left(\frac{T-T_{sol}}{T_{liq}-T_{sol}}\right)^{b-1}\frac{\partial T}{\partial t}\right|. \tag{15}$$

We approximate $\nabla^2 T$ as $(T_{liq}-T_{sol})/H^2$, where H is the thickness of the magma body.

The cooling rate becomes

$$\left|\frac{\partial T}{\partial t}\right| \simeq \underbrace{\frac{c\left(T_{liq}-T_{sol}\right)}{L}}_{St'}\frac{\kappa\left(T_{liq}-T_{sol}\right)}{H^2 b}\left(\frac{T-T_{sol}}{T_{liq}-T_{sol}}\right)^{1-b}, \tag{16}$$

where St' is a Stefan number (ratio of sensible to latent heat). We define a first timescale τ_1 which is a measure of the time required for a body to cool and crystallize,

$$\tau_1 \equiv \frac{T_{liq}-T_{sol}}{\left|\frac{\partial T}{\partial t}\right|}. \tag{17}$$

According to our model, this cooling timescale is

$$\tau_1 \simeq \frac{bH^2}{St'\kappa}\left(\frac{T-T_{sol}}{T_{liq}-T_{sol}}\right)^{b-1} \tag{18}$$

and becomes very long as $T \to T_{sol}$.

For a cooling volume to get more homogeneous in temperature, the cooling rate must be a function of temperature and must also decrease as the solidus temperature is approached, allowing patches with different initial temperature to converge towards T_{sol}. We will refer to the convergence timescale for patches starting with different temperatures as the homogenization timescale τ_2. We define this timescale as

$$\tau_2 \equiv \left|\frac{\frac{\partial T}{\partial t}}{\frac{\partial^2 T}{\partial t^2}}\right|. \tag{19}$$

An analogy to momentum helps us to understand this choice for τ_2. The distance between two objects following the exact same trajectory described by the position x and traveling at velocities that only depend on their respective position will evolve as a consequence of the ratio of the local velocity and acceleration (first derivative of position divided by the second derivative of position). The second derivative of the temperature is easily derived from above

$$\tau_2 \simeq \left(\frac{T-T_{sol}}{T_{liq}-T_{sol}}\right)^{b}\frac{bH^2}{St'\kappa(1-b)}. \tag{20}$$

First, we see that, unlike τ_1, τ_2 does not diverge close to the solidus temperature but approaches zero. As different patches cool to the eutectic temperature, the temperature of the whole system converges to the solidus temperature, and $\tau_2 \to 0$. Any other timescale will become greater than τ_2 if it does not converge faster to zero, implying that homogenization of the temperature field is inevitably the dominant trend for a crystallizing eutectic melt.

To illustrate the buffering effect of latent heat, we use a combination of the stagnant-lid convection cooling model of Section 2 (below 45% crystals) with a lattice Boltzmann method to model heat diffusion with solidification (beyond 45%). More details on the lattice Boltzmann model for heat diffusion and solidification can be found in Huber et al. (2008). The choice of 45 vol.% crystals to stop the stagnant-lid convection cooling model is somewhat arbitrary but is within the range of crystallinities where heat conduction is expected to dominate. Therefore, we need to use another model to track the spatial and temporal evolution of both temperature and crystallinity in a crystal-rich magma chamber (from 45 vol. % crystals up to fully crystallized) that neglects heat advection. Fig. 6 shows histograms of the time that the magma chamber spends at various average temperatures and crystallinities during its cooling history (closed system) for different melt fraction–temperature relationships (Eq. (13) with $b=1$, 0.5 and 0.1). As the exponent decreases to zero, the latent heat buffering becomes stronger and occurs over a narrower range of temperatures (Fig. 6f) at which the magma chamber spends the majority of its time. This effect is less perceptible for the average crystallinity (Fig. 6e) because for small exponents b, at high χ (>0.5), a small decrease in temperature leads to a large increase in crystallinity.

The calculations for the cooling history show a strong dependence on the eutectic exponent b illustrating the importance of latent heat buffering on the evolution of temperature and crystallinity in silicic magmas. Fig. 7 shows the evolution of the temperature and melt fraction ($f=1-\chi$) using the solidification–diffusion model for two different times, the time is reset to zero when the crystallinity reaches 0.45 and the heat transfer is assumed to occur by conduction. The initial condition (cooling history up to $\chi=0.45$) is again calculated with the cooling model described in Section 2 and Appendix A, as we assumed for Fig. 6. The shaded area represents the initial size of the magma chamber. At the initiation of these calculations, we perturb the temperature field at the base of the chamber by 20 °C to simulate the effect of latent heat buffering on heterogeneities or the reheating of the basal part of the chamber. This temperature heterogeneity is associated with a larger crystallinity heterogeneity at low values of b because of the narrower range of temperatures over which the crystallinity varies close to the solidus (here $T_{sol}/T_{liq}=0.7$). For the case where $b=0.1$, the perturbation in temperature and crystallinity is large enough to allow the lower part of the magma chamber to convect. Restarting convection is not taken into account. The convective flux, however, will not affect the existence of the mushification process as described by Eq. (14), and the latent heat buffering will remain relevant. Fig. 7a shows that the thermal buffering for $b=0.1$ allows the non-fully crystallized part of the magma chamber to remain at a constant temperature for at least 6 ka, whereas for $b>0.1$, the temperature within the chamber show larger spatial variations and a stronger time dependence. This effect is even stronger for the crystallinity profiles (Fig. 7b), where after 6.5 ka, the profile for $b=0.1$ shows a nearly constant crystallinity (about 30%) across the whole chamber even though the temperature dependence of the melt fraction is much stronger. These calculations show that for a eutectic phase diagram where the bulk of the crystallization occurs within a narrow range of temperature above the solidus, the magma chamber at first cools faster due to convection at low crystallinities and then becomes trapped close to the solidus for the major part of its supra-solidus cooling. During this latest phase (mushification), both temperature and crystallinity heterogeneities have more time to diffuse away.

In a more general approach, the melt fraction does not only depend on temperature, but also on chemical composition. We simplify the following argument by introducing a single new variable C representing the composition of the melt. In Eq. (8), we can substitute

$$\frac{\partial f}{\partial t} \to \frac{\partial f}{\partial T}\frac{\partial T}{\partial t} + \frac{\partial f}{\partial C}\frac{\partial C}{\partial T}\frac{\partial T}{\partial t} = \frac{\partial T}{\partial t}\underbrace{\left(\frac{\partial f}{\partial T} + \frac{\partial f}{\partial C}\frac{\partial C}{\partial T}\right)}_{\frac{df}{dT}} \tag{21}$$

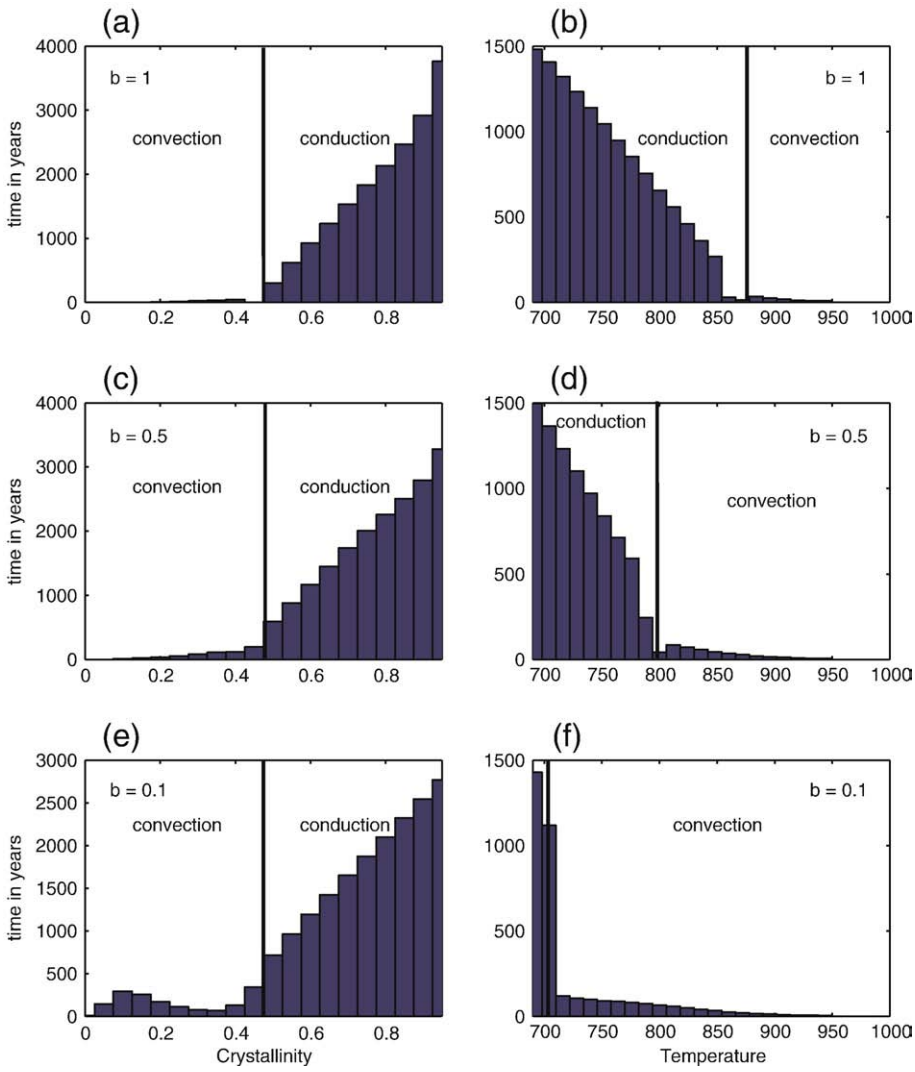

Fig. 6. (a–c–e) Histograms of the time spent by the magma chamber at different averaged crystallinities for different exponent *b*. The magma chamber cools as a closed system as described in Section 2. The cooling model described in Appendix A is used until the crystallinity reaches 0.45 (represented by the vertical solid lines). The subsequent evolution of the magma chamber is calculated with a diffusion–solidification lattice Boltzmann model (see Appendix A for more details). (b–d–f) Histograms of the time spent by the magma chamber at different averaged temperatures for the same three melt fraction–temperature exponents.

The introduction of a dependence on composition in the melt fraction introduces two new timescales similar to τ_1 and τ_2 from the contribution of the second term in the right-hand side of Eq. (21). Because of the difference between the thermal diffusion and the much slower chemical diffusion timescales, the compositional equivalent of τ_1 and τ_2 obtained from $(\partial f/\partial C)(\partial C/\partial T)$ will always be several orders of magnitude larger than the thermal τ_1 and τ_2, and will not play any significant role in determining the rate of homogenization.

5. The case of the Fish Canyon magma body

In order to illustrate how convection and mushification processes operate in an upper crustal magma chamber, we use the Fish Canyon magma body as a natural example. This large (>5000 km^3) dacitic system produced one of the largest known ignimbrites; the Fish Canyon Tuff (FCT). This ignimbrite is remarkable for its thermal and chemical homogeneity (Whitney and Stormer, 1985; Bachmann et al., 2002; Charlier et al., 2007) at the whole-rock scale. Temperature variations based on Fe–Ti oxides and Quartz–Magnetite oxygen isotope thermometry is less than 30 °C and the silica content of pumice varies by less than 2 wt.% SiO_2 throughout the entire deposit (Bachmann and Dungan, 2002; Bachmann et al., 2002; Ghiorso and Evans, 2008). In contrast, the system is very heterogeneous at the crystal scale and chemically zoned minerals attest to an open system behavior. In particular, some biotite crystals are inherited from the Precambrian wall rocks (Charlier et al., 2007). As these biotites must come from the edges of the reservoir and are now found well dispersed throughout the magma body (as independent crystals not enclosed in xenoliths), an efficient stirring event has occurred after wall rock assimilation. Diffusion modelling of Sr in biotite suggests that assimilation and stirring took place within a 1–10 ka period prior to eruption (Charlier et al., 2007).

A plausible source for the stirring is a rejuvenation event that occurred prior to the Fish Canyon Tuff eruption. Textural and geochemical data suggest that the magma has been reheated and partially remelted some time before eruption by the underplating of hot, more mafic magma (Bachmann and Dungan, 2002; Bachmann et al., 2002; Parat et al., 2008). In addition, the underplating, hot mafic magma was volatile-rich (Parat et al., 2008) and likely released a buoyant fluid phase, which added a source of convective instability at the base of the magma chamber (Bachmann and Bergantz, 2006). Further, magma stirring by bubble rise may leave a gradient in bubble concentration (e.g., Ruprecht et al., 2008), but such a gradient would not be preserved in erupted deposits.

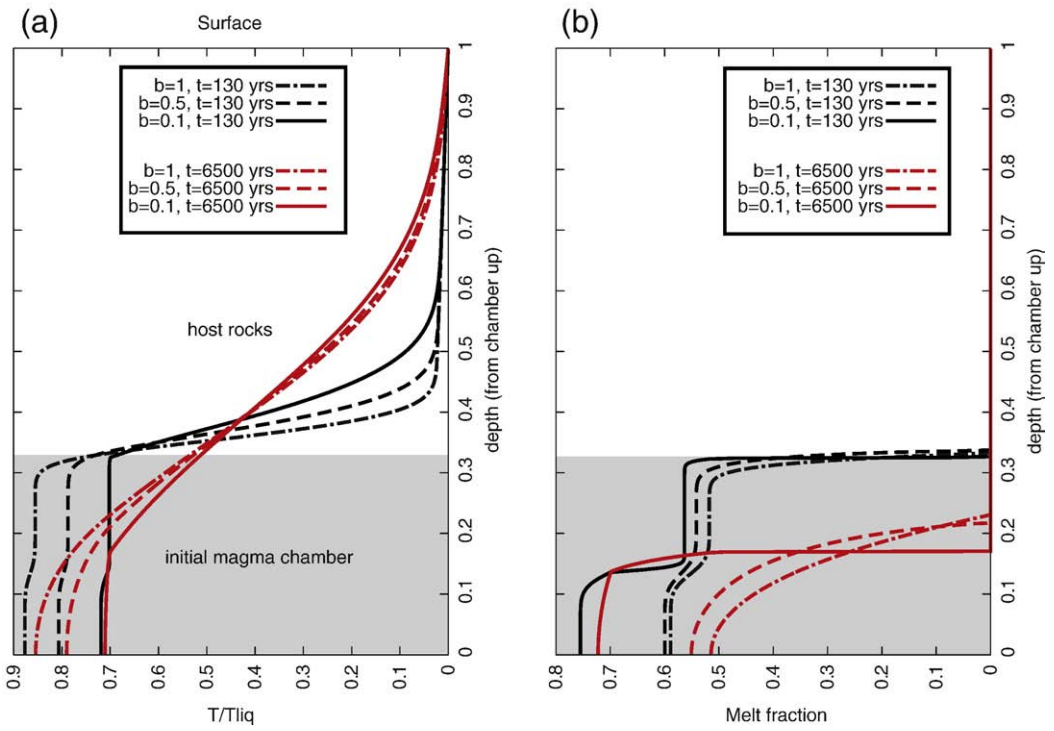

Fig. 7. Results of the solidification–diffusion lattice Boltzmann calculations for the evolution of the temperature and crystallinity profiles. (a) Normalized temperature profiles across the magma chamber (from 0 to 0.33 on *x*-axis) and the overlying host rocks for two distinct times and different melt fraction–temperature exponents. The initial condition is the result of the calculations when the magma chamber average crystallinity reaches 0.45 using the cooling model presented in Section 2. For all calculations the normalized temperature of the solidus is set to 0.7. We add a temperature perturbation in the bottom part of the chamber of 20 °C to illustrate the evolution of heterogeneities in a mush close to the solidus for different "eutectic" behaviors. (b) Equivalent profiles for the melt fraction. The effect of the temperature perturbation at the base of the chamber is greatest for low *b* as a difference in 20° close to the solidus corresponds to a large difference in crystallinity (about 20 vol.%). For the case where $b = 0.1$, the perturbation in temperature and crystallinity is large enough to allow the lower part of the magma chamber to convect. This is not taken into account, however the convective flux will not affect the existence of the mushification process as Eq. (14) which introduced the latent heat buffering remains relevant.

In order to explain the characteristics of the Fish Canyon magma body, we propose the following conceptual model. (1) To alleviate the room problem inherent to the presence of a large magma reservoir in the upper crust, we concur that the magma body had to grow incrementally (e.g., Petford et al., 2000). Silicic increments fairly similar in composition to the bulk reservoir were stored into the magma chamber, but more mafic, denser additions were gravitationally blocked by the silicic reservoir and acted as heat source for the overlying silicic magma. (2) The mushification process kept the system in a state of high crystallinity ("crystal mush") for most of its life, as new magma inputs quickly caught up in temperature and crystallinity with the rest of the reservoir. (3) The episodic injections of more mafic magmas, underplating the growing silicic reservoir, allowed periodic reactivation of the magma chamber by reheating and gas sparging from below (Bachmann and Bergantz, 2006). Such a reactivation event occurred shortly before eruption, triggering partial melting of the crystalline framework, late-stage stirring (as inferred from the biotites), and ultimately the eruption of a significant portion of the mush.

The Fish Canyon magma body has the archetypal upper crustal composition. Its major and trace element concentrations are nearly identical to the average composition of the upper crust, as determined by Taylor and McLennan (1985). It is also very similar to large granodiorite batholiths such as those found in the Sierra Nevada (e.g., Half Dome Granodiorite, Bateman and Chappell, 1979). We believe that the scenario outlined here may be common in the evolution of large silicic magma bodies that build the upper crust.

6. Concluding remarks

Mixing efficiency is a strong function of *Ra* (and hence *Re*) number (Oldenburg et al., 1989; Bergantz and Ni, 1999; Jellinek and Kerr, 1999; Coltice and Schmalzl, 2006). However, in cases where convection is chaotic, mixing can also be efficient even at small *Re* numbers, if enough time is allowed for the stirring to occur. We have argued here that the relevant variable to quantify mixing is the cumulative amount of strain that follows the creation of a discrete heterogeneity. It is therefore the number of overturns and not a given Reynolds number that is critical to attain homogeneity by convective stirring.

The stirring efficiency for crystallinity, composition and/or temperature fields also depends on the source of buoyancy that generates convection. Convective currents in magmas are mainly driven by two buoyancy sources: (1) phase changes in a cooling/heating environment, and (2) density changes due to compositional differences. Typical scenarios in magma reservoirs, either convective motion due to the introduction of low density gas or magma from below, or falling of dense crystal plumes from the roof, will lead to a stable, stratified situation in one overturn (Oldenburg et al., 1989; Bergantz and Ni, 1999; Jellinek and Kerr, 1999). Dense crystals or more mafic magmas tend to accumulate in the lower part of the magma reservoir, while low density phases (silicic melt and gas bubbles) gather near the roof. In such scenarios, the material from the boundary layers have different physico-chemical characteristics (temperature, crystallinity or composition) from the bulk of the convecting magma, and will always lead to addition of new heterogeneities as boundary layers detach.

As expected, most magmatic units are heterogeneous at many scales, implying that complex mixing and unmixing occurs while the magmas interact with each other and the surrounding crust (Table 2). However, crystal-rich, large silicic ignimbrites (the Monotonous Intermediates) and many granitoid plutons are compositionally homogeneous at the hand sample scale. These units are the most viscous magmas the Earth produces, and therefore the least likely to be mixed by high *Re*

Table 2
Effect of the different processes on the evolution of heterogeneities in a magmatic system.

Process	Homogenization	Heterogenization	Fields affected
Assimilation	–	x	T, χ, C_M and C_t
Replenishment	–	x	T, χ, C_M and C_t
Crystal–liquid separation	–	x	χ, C_M and C_t
Convection	x	x	T, χ, C_M and C_t
Mushification	x	–	T and χ

C_M and C_t refer respectively to major and trace elements composition.

convection. These paradoxically homogeneous, crystal-rich, silicic systems require: (1) the growth of large silicic reservoirs by incremental additions of compositionally similar magmas. (2) A mushification stage, induced by latent heat buffering close to the haplogranite eutectic, that leads to extended storage at high crystallinity (χ>0.5 crystals). As melt viscosity is high and crystals small, heterogenization by crystal–liquid separation is slow, and large areas have little to no gradients for long periods of time. Moreover, these mushes are periodically intruded by hotter, more mafic magmas. These mafic magmas cannot easily penetrate into the overlying mush due to their higher densities, but will liberate heat and gas. Therefore, these underplating events lead to self-mixing, by reheating and partially remelting of the crystalline framework. This rejuvenation process will be favoured by the decrease in melt viscosity as a function of pressure that is expected in volatile-saturated mushes. Late stirring is also required by the distribution of xenocrysts (biotite, zircons) throughout large silicic magma bodies (e.g., Yoshinobu et al., 2003; Hawkins and Wiebe, 2004; Charlier et al., 2007; Miller et al., 2007) and can be attributed to a combined effect of thermal rejuvenation and injection of buoyant gas from the underplating magma.

Acknowledgements

C.H. and M.M were supported by NSF EAR 0608885 and the Larsen Fund. Swiss NSF grant #200021-111709 provided support to O.B during the completion of this paper. The authors would like to thank the editor T.M. Harrison and two anonymous reviewers for their constructive comments. This paper has been a stirring experience for us, and we are thankful to George Bergantz and Joe Dufek for continuous support and numerous discussions on the topics expressed in this paper.

Appendix A. Cooling model

This model assumes no hydrothermal circulation which would enhance the cooling of the magma body. The increased heat transfer associated with the circulation of fluids can be parameterized with a Nusselt number in Eq. (1). The Nusselt number Nu is defined as the ratio of diffusion to advection timescales for heat transfer. As expected, calculations including the simplified effect of hydrothermal circulation basically rescaled the time of cooling by a factor proportional to Nu^{-1} but did not affect the general cooling trend.

The magma temperature in the convecting layer is calculated using the following scheme: q_{out} has to match the heat flux out of the magma chamber cooling by convection and the heat released by crystallization. Following Davaille and Jaupart (1993), the heat flux for a convectively cooling system in the stagnant lid regime is given by

$$q_s = -0.47 k_m \left(\frac{\alpha g}{\kappa_m \nu_m}\right)^{1/3} \left(-\frac{\mu_m(T_m)}{d\mu_m/dT(T_m)}\right)^{4/3} \quad (22)$$

where the expansion coefficient α takes into account both thermal expansion α_T and crystallinity changes (ρ_c and ρ_m are respectively the density of crystals and melt)

$$\alpha = \frac{\rho_c - \rho_m}{\rho_0}\frac{\partial \chi}{\partial T} + \alpha_T. \quad (23)$$

ρ_0 is the density of the melt at a reference temperature (T_i, in this case). In Eq. (22), T_m, κ_m, k_m, ν_m and μ_m are the temperature of the convecting magma, the heat diffusivity, the thermal conductivity, the kinematic and dynamic viscosity of the magma. The thickness of the stagnant lid δ is given by Davaille and Jaupart (1994)

$$\delta = k_m \frac{\Delta T - \Delta T_e}{q_s} \quad (24)$$

where ΔT is the temperature drop across the whole boundary layer ($\Delta T = T_m - T_{roof}$) and ΔT_e is the temperature difference driving the convection (Davaille and Jaupart, 1993, 1994)

$$\Delta T_e = 2.24\left(-\frac{\mu(T_m)}{d\mu/dT(T_m)}\right). \quad (25)$$

The viscosity of the magma is calculated from

$$\mu(T) = \mu_0 \exp\left[\frac{Q}{RT_i}\left(\frac{T_{ini}}{T} - 1\right)\right]\left[1 + 0.75\frac{\chi(T)/\chi_{cr}}{1-\chi(T)/\chi_{cr}}\right]^2 \quad (26)$$

where Q is the activation energy (500 kJ) and R is the gas constant. As the crystallinity of the system evolves with the temperature of the magma, the latent heat released will also contribute to the thermal balance with a contribution $\rho_c V L \dot{\chi}/S$. ρ_c, V, L, $\dot{\chi}$ and S are respectively the density of the crystalline phase, the volume of the chamber, the latent heat, the crystallization rate and the surface area of the chamber's roof. This must be added to the convective heat flux of Eq. (22).

Setting the total heat flux out of the magma body to the value determined by the heat diffusion equation solved for the host rock, we can determine the temperature in the convecting magma for the next time step (using a Newton–Raphson solver).

At each time step, we can calculate the evolution of the Rayleigh number in the chamber

$$Ra(t) = \frac{\rho_0 \alpha \Delta T_e g H^3}{\kappa \mu(t)} \quad (27)$$

where H is the thickness of the magma body.

References

Bachmann, O., Bergantz, G.W., 2006. Gas percolation in upper-crustal magma bodies as a mechanism for upward heat advection and rejuvenation of silicic crystal mushes. J. Volcanol. Geotherm. Res. 149, 85–102.
Bachmann, O., Dungan, M.A., 2002. Temperature-induced Al-zoning in hornblendes of the fish Canyon magma, Colorado. Am. Mineral. 87, 1062–1076.
Bachmann, O., Dungan, M.A., Lipman, P.W., 2002. The Fish Canyon magma body, San Juan volcanic field, Colorado: rejuvenation and eruption of an upper crustal batholith. J. Petrol. 43, 1469–1503.
Bachmann, O., Miller, C.F., de Silva, S., 2007. The volcanic–plutonic connection as a stage for understanding crustal magmatism. J. Volcanol. Geotherm. Res. 167, 1–23.
Bateman, P.C., Chappell, B.W., 1979. Crystallization, fractionation, and solidification of the Tuolumne Intrusive Series, Yosemite National Park, California. GSA Bull. 90, 465–482.
Bergantz, G.W., 1992. Conjugate solidification and melting in multicomponent open and closed systems. Int. J. Heat Mass Transfer 35 (2), 533–543.
Bergantz, G.W., Ni, J., 1999. A numerical study of sedimentation by dripping instabilities in viscous fluids. Int. J. Multiph. Flow 25, 307–320.
Bowen, N.L., 1992. The Evolution of the Igneous Rocks. Dover Publications, New York.
Burgisser, A., Bergantz, G.W., Breidenthal, R.E., 2005. Addressing complexity in laboratory experiments: the scaling of dilute multiphase flows in magmatic systems. J. Volcanol. Geotherm. Res. 141, 245–265.
Campbell, I.H., Taylor, S.R., 1988. No water, no granites no oceans, no continents. Geophys. Res. Lett. 10, 1061–1064.
Carrigan, C.R., 1988. Biot number and thermos bottle effect: implications for magma-chamber convection. Geology 16, 771–774.

Caricchi, L., Burlini, L., Ulmer, P., Gerya, T., Vassalli, M., Papale, P., 2007. Non-Newtonian rheology of crystal-bearing magmas and implications for magma ascent dynamics. Earth Planet. Sci. Lett. 264, 402–419.
Champallier, R., Bystricky, M., Arbaret, L., 2008. Experimental investigation of magma rheology at 300 MPa: from pure hydrous melt to 76 vol.% of crystals. Earth Planet. Sci. Lett. 267, 571–583.
Charlier, B.L.A., Bachmann, O., Davidson, J.P., Dungan, M.A., Morgan, D., 2007. The upper crustal evolution of a large silicic magma body: evidence from crystal-scale Rb/Sr isotopic heterogeneities in the Fish Canyon Magmatic System, Colorado. J. Petrol. 48, 1875–1894.
Chen, C.F., Turner, J.S., 1980. Crystallization in double-diffusive system. J. Geophys. Res. 85, 2573–2593.
Christiansen, E.N., 2005. Contrasting processes in silicic magma chambers: evidence from very large volume ignimbrites. Geol. Mag. 142, 669–681.
Coltice, N., Schmalzl, J., 2006. Mixing times in the mantle of the early Earth derived from 2-D and 3-D numerical simulations of convection. Geophys. Res. Lett. 33 (L23304). doi:10.1029/2006GL027707.
Couch, S., Sparks, R.S.J., Carroll, M.R., 2001. Mineral disequilibrium in lavas explained by convective self-mixing in open magma chambers. Nature 411, 1037–1039.
Davaille, A., Jaupart, C., 1993. Transient high-Rayleigh-number thermal convection with large viscosity variations. J. Fluid Mech. 253, 141–166.
Davaille, A., Jaupart, C., 1994. Onset of thermal convection in fluids with temperature-dependent viscosity: application to the oceanic mantle. J. Geophys. Res. 99, 19853–19866.
Eichelberger, J.C., Chertkoff, D.G., Dreher, S.T., Nye, C.J., 2000. Magmas in collision: rethinking chemical zonation in silicic magmas. Geology 28, 603–606.
Ghiorso, M.S., Evans, B.W., 2008. Thermodynamics of rhombohedral oxide solid solutions and a revision of the Fe–Ti oxide geothermometer and oxygen-barometer. Am. J. Sci. 308, 957–1039.
Ghiorso, M.S., Sack, R.O., 1995. Chemical mass transfer in magmatic processes IV: a revised and internally consistent thermodynamic model for the interpolation and extrapolation of liquid–solid equilibria in magmatic systems at elevated temperatures and pressures. Contrib. Mineral. Petrol. 119, 197–212.
Grout, F.F., 1918. Two phase convection in igneous magmas. J. Geol. 26, 481–499.
Hawkins, D.P., Wiebe, R.A., 2004. Discrete stoping events in granite plutons; a signature of eruptions from silicic magma chambers? Geology 32, 1021–1024.
Hildreth, W., 1981. Gradients in silicic magma chambers: implications for lithospheric magmatism. J. Geophys. Res. 86, 10153–10192.
Hoover, S.R., Cashman, K.V., Manga, M., 2001. The yield strength of subliquidus basalts experimental results. J. Volcanol. Geotherm. Res. 107, 1–18.
Huber, C., Parmigiani, A., Chopard, B., Manga, M., Bachmann, O., 2008. Lattice Boltzmann model for melting with natural convection. Int. J. Heat Fluid Flow 29, 1469–1480.
Huppert, H.E., Sparks, R.S.J., Turner, J.S., 1982. Effects of volatiles on mixing in calcalkaline magma systems. Nature 332, 554–557.
Jellinek, A.M., Kerr, R.C., 1999. Mixing and compositional stratification produced by natural convection: 2. Applications to the differentiation of basaltic and silicic magma chambers and komatiite lava flows. J. Geophys. Res. 104, 7203–7218.
Jellinek, A.M., Kerr, R.C., Griffiths, R.W., 1999. Mixing and compositional stratification produced by natural convection: 1. Experiments and their applications to Earth's core and mantle. J. Geophys. Res. 104, 7183–7201.
Koyaguchi, T., Kaneko, K., 1999. A two-stage thermal evolution model of magmas in continental crust. J. Petrol. 40, 241–254.
Koyaguchi, T., Kaneko, K., 2001. Thermal evolution of silicic magma chambers after basalt replenishment. Trans. R. Soc. Edinb. 91, 47–60.
Koyaguchi, T., Hallworth, M.A., Huppert, H.E., Sparks, R.S.J., 1990. Sedimentation of particles from a convecting fluid. Nature 343, 447–450.
Lindsay, J.M., Schmitt, A.K., Trumbull, R.B., de Silva, S.L., Emmermann, R., 2001. Magmatic evolution of the La Pacana caldera system, Central Andes, Chile: compositional variation of the two cogenetic, large-volume felsic ignimbrites. J. Petrol. 42, 459–486.
Manga, M., 1996. Mixing of heterogeneities in the mantle: effects of viscosity differences. Geophys. Res. Lett. 23, 403–406.
Marsh, B.D., 1981. On the crystallinity, probability of occurrence, and rheology of lava and magma. Contrib. Mineral. Petrol. 78, 85–98.
Marsh, B.D., 1989a. Magma chambers. Annu. Rev. Earth Planet. Sci. 17, 439–474.
Marsh, B.D., 1989b. On convective style and vigor in sheet-like magma chambers. J. Petrol. 30, 479–530.
Martin, D., Nokes, R., 1989. A fluid-dynamical study of crystal settling in convecting magmas. J. Petrol. 30, 1471–1500.
McBirney, A.R., 1980. Mixing and unmixing of magmas. J. Volcanol. Geotherm. Res. 7, 357–371.
McBirney, A.R., Baker, B.H., Nilson, R.H., 1985. Liquid fractionation. Part 1: basic principles and experimental simulations. J. Volcanol. Geotherm. Res. 24, 1–24.
Miller, J.S., Matzel, J.E.P., Miller, C.F., Burgess, S.D., Miller, R.B., 2007. Zircon growth and recycling during the assembly of large, composite arc plutons. J. Volcanol. Geotherm. Res. 167, 282–299.
Oldenburg, C.M., Spera, F.J., Yuen, D.A., Sewell, G., 1989. Dynamic mixing in magma bodies: theory, simulations, and implications. J. Geophys. Res. 94, 9215–9236.
Olson, P., Yuen, D.A., Balsiger, D., 1984. Convective mixing and the fine structure of mantle heterogeneity. Phys. Earth Planet. Inter. 36, 291–304.
Ottino, J.M., 1990. Mixing, chaotic advection, and turbulence. Annu. Rev. Fluid Mech. 22, 207–253.
Parat, F., Holtz, F., Feig, S., 2008. Pre-eruptive conditions of the Huerto Andesite (Fish Canyon System, San Juan Volcanic Field, Colorado): influence of volatiles (C–O–H–S) on phase equilibria and mineral composition. J. Petrol. 49 (5), 911–935.
Petford, N., 2003. Rheology of granitic magmas during ascent and emplacement. Annu. Rev. Earth Planet. Sci. 31, 399–427.
Petford, N., Cruden, A.R., McCaffrey, K.J.W., Vigneresse, J.-L., 2000. Granite magma formation, transport and emplacement in the Earth's crust. Nature 408, 669–673.
Philpotts, A.R., Shi, J., Brustman, C., 1998. Role of plagioclase crystal chains in the differentiation of partly crystallized basaltic magma. Nature 395, 343–346.
Ruprecht, P., Bergantz, G.W., Dufek, J., 2008. Modeling of gas-driven magmatic over-turn: tracking of phenocryst dispersal and gathering during magma mixing. Geochem. Geophys. Geosyst. 9 (7). doi:10.1029/2008GC002022.
Saar, M.O., Manga, M., 2002. Continuum percolation for randomly oriented soft-core prisms. Phys. Rev. E 65 (056131).
Scaillet, B., Holtz, F., Pichavant, M., 1998. Phase equilibrium constraints on the viscosity of silicic magmas 1. Volcanic–plutonic comparison. J. Geophys. Res. 103 (B11), 27257–27266.
Sparks, R.S.J., 1990. Comment on "Crystal capture, sorting, and retention in convecting magma" by Marsh. B.D. Geol. Soc. Amer. Bull. 102, 847–848.
Sparks, R.S.J., Marshall, L.A., 1986. Thermal and mechanical constraints on mixing between mafic and silicic magmas. J. Volcanol. Geotherm. Res. 29, 99–124.
Sparks, R.S.J., Huppert, H.E., Turner, J.S., 1984. The fluid dynamics of evolving magma chambers. Philos. Trans. R. Soc. Lond. 310, 511–534.
Taylor, S.R., McLennan, S.M., 1985. The Continental Crust: Its Composition and Evolution. Blackwell, Cambridge, Mass. 312 pp.
Turcotte, D.L., Schubert, G., 2002. Geodynamics, 2nd ed. Cambridge University Press.
Vigneresse, J.-L., Barbey, P., Cuney, M., 1996. Rheological transitions during partial melting and crystallization with application to felsic magma segregation and transfer. J. Petrol. 37, 1579–1600.
Whitney, J.A., Stormer Jr., J.C., 1985. Mineralogy, petrology, and magmatic conditions from the Fish Canyon Tuff, central San Juan volcanic field, Colorado. J. Petrol. 26, 726–762.
Yoshinobu, A.S., Fowler, T.K., Paterson, S.R., Llambias, E., Tickyj, H., Sato, A.M., 2003. A view from the roof: magmatic stoping in the shallow crust, Chita pluton, Argentina. J. Struct. Geol. 25, 1037–1048.